Revista Mexicana de Astronomía y Astrofísica, **43**, 59–87 (2007)

PHYSICAL MECHANISMS THAT SHAPE THE MORPHOLOGIES OF EXTRAGALACTIC JETS

L. Zaninetti

Dipartimento di Fisica Generale, Università degli Studi di Torino, Italy

Received 2006 March 2; accepted 2006 October 10

RESUMEN

Se sugieren 5 métodos analíticos para encontrar una ley que caracterice el decremento de la velocidad a lo largo del chorro. Los 2 primeros son modelos simples que examinan la variación de la velocidad en presencia de la resistencia de Newton o de Stoke. Se resuelve la ecuación que representa la conservación del momento a lo largo de un sector piramidal desde un punto de vista analítico (tercer modelo). La aplicación de la conservación del flujo del momento total nos permite deducir la velocidad de la galaxia como función del tiempo para velocidades clásicas (cuarto modelo) y para velocidades relativistas (quinto modelo). La variación de la velocidad a lo largo del chorro combinada con una adecuada composición de la velocidad de precesión del chorro, con la velocidad rotacional de la galaxia y con la dispersión de velocidades de la galaxia en el cúmulo nos permite trazar el patrón geométrico de las fuentes de radio con cabeza y cola. La aplicación de la teoría/código desarrollado a las radiogalaxias NGC1265, NGC4061, NGC326, y Cygnus A nos da una dispersión de velocidades aproximada de la galaxia central en la dirección perpendicular al chorro. Introducimos una transición desde las galaxias cabeza-cola a las clásicas radiogalaxias dobles como función del incremento de la potencia mecánica del chorro.

ABSTRACT

In order to find a law characterising the decrease of velocity along a jet, five analytical methods are suggested. The first two simple models examine the variation of velocity in the presence of Newton's or Stoke's resistance. The equation that represents the conservation of the momentum along a pyramidal sector is solved from an analytical point of view (third model). The application of the conservation of the total momentum flux allows us to deduce the velocity of the galaxy as a function of time for classical velocities (fourth model) and relativistic velocities (fifth model). The variation of velocity along the jet combined with an adequate composition of jet precession velocity, rotational velocity of the galaxy, and galaxy velocity dispersion in the cluster allows us to trace the geometrical pattern of the head-tail radio sources. Application of the developed theory/code to the radio galaxies NGC1265, NGC4061, NGC326, and Cygnus A gives the central galaxy's approximate dispersion velocities in the direction perpendicular to the jet. A transition from head–tails to classical double radio galaxies as a function of the increasing jet's mechanical power is introduced.

Key Words: **GALAXIES: JETS — RADIO CONTINUUM: GALAXIES**

1. INTRODUCTION

The extragalactic radio sources are classified on the basis of the position of the brightest radio emitting regions with respect to the channel: FR-I have hot spots that are more distant from the nucleus (typical example Cygnus A), FR-II radio galaxies have emission uniformly distributed along the channel (typical example 3C449). The physical parameter that governs this classification is the radiated power, the more powerful radio galaxies being classified as FR II, see Fanaroff & Riley (1974) for details. The classification then becomes more complicated in the presence of complex morphologies and two classifications are introduced: NAT (Narrow Angle Tail) and WAT (Wide Angle Tail). But a closer look at NGC 1265 reveals that the angle subtended by the two channels is not so "narrow", see Figure 1 of Odea & Owen (1986); possibly, in this case a distinction should be made between internal regions of the channel where the patterns are similar and the extended regions where conversely the division in WAT and NAT is more evident.

For more details on the classification scheme the interested reader is advised to refer to the book by De Young (2002). The X-ray observations of the Galactic black hole XTE J1118+480 are consistent with extended jets being the source of the hard X-ray flux. In this hypothesis the disc would then simply represent a small solid angle as seen from the emission region, see Miller et al. (2002). This point of view is not new and has been explored by Mendoza, Hernández, & Lee (2005) who suggested a unified model for quasars and mu-quasars. In general, the shapes seem to be independent from (or weakly correlated to) the cluster parameters, such as physical position in the cluster, number of galaxies, cluster richness, cluster morphology and x-ray emission. Some of the models that can explain the bending of the jets will now be briefly reviewed:

- The *geometrical models* started with Jaffe & Perola (1973) where two models were developed to explain the formation of "tailed" radio sources like 3C 129. They continued inserting precession and relativistic effects in SS433, see Hjellming & Johnston (1982). An analytical model was presented for the evolution of a powerful double radio source on a small scale, see Alexander (2000).

- *Euler's equation model*, where bending is produced by the ram pressure $\rho_{ICM} V_j^2$ of the intra-cluster medium, is analysed by Burns & Owen (1980) in order to explain the structure of 1638+538 (4C53.57), and by Venkatesan et al. (1994) in order to understand the behaviour of NAT in poor clusters of galaxies. Further, a hydro-dynamical code was built in order to explain the NAT sources, see Norman, Balsara, & O'Dea (1994). From an observational point of view it is interesting to note that the velocities of the NAT galaxies are inadequate for producing the ram pressure necessary to bend the radio jets, see Bliton et al. (1998).

- The *slingshot ejection model* consists in the ejection of black holes from the host galaxy: the bending is obtained from the oscillations about the center of the merged galaxy, see for example Valtonen & Kotilainen (1989).

- The 3-dimensional magneto-hydrodynamic (MHD) simulations, based on the Sweeping Magnetic-Twist model Nakamura, Uchida, & Hirose (2001), produce a wiggly structure of AGN radio jets.

- The interaction of a jet with a stratified cloud, see Raga & Cantó (1996), or with a spherically symmetric pressure stratification, see Cantó & Raga (1996), can lead to a final configuration in which the jet has bored a hole through the cloud, or large deflections are obtained.

- A jet can generate an internal shock wave by adopting either a non-relativistic framework, see Icke (1991) or a relativistic framework, see Mendoza & Longair (2002).

- From a relativistic point of view Mendoza & Longair (2001) showed that bending relativistic jets is much more difficult than bending non-relativistic ones. This is the reason why most FR-II radio galaxies appear straight.

The already cited models concerning the bending leave a series of questions unanswered or partially answered:

- Is it possible to deduce a law of motion in the presence of viscosity in laminar and turbulent jets?

- Is it possible to trace the jet velocity on the basis of physical parameters such as linear density of energy of the radio source and constant density of the IGM (Inter Galactic Medium)?

- Is it possible to develop a consistent theory in which, at a given time, the jet opening angle increases abruptly?
- Is it possible to include relativistic effects in turbulent jets that generalise the work made by Raga & Cantó (1996) and Cantó & Raga (1996) on the interaction between a jet and a stratified cloud?
- Once the main jet trajectory is obtained, could other kinematical components be added such as jet precession, galaxy rotation and galaxy bulk velocity?
- Does the developed theory match the observed patterns traced by the radio sources?
- Could the transition FR-I ⇒ FR-II be simulated by increasing the total jet luminosity?

In order to answer these questions in Section 2 the equations of motion are derived in the presence of Stoke's law of resistance, Newton's law of resistance and turbulent eddy viscosity. Some analytical computations on the momentum conservation in an extra-galactic pyramidal sector advancing in a surrounding medium are developed in Section 3. In Section 4 the theory of the two-phase beam is set up. The theory of relativistic turbulent jets is developed in Section 5. The theory for the composition of the velocities in a head-tail radio source is developed in Section 6. The application of the developed theory to well-specified radio sources such as NGC1265, NGC4061, NGC326 and Cygnus A is reported in Section 7. A power transition is simulated in Section 7.5 replacing the energy with the total power in the law of motion. The theory of the Kelvin-Helmholtz instabilities is reviewed and implemented on the radio-sources in Section 9.

2. VISCOSITY MODELS

When a laminar jet moves through the IGM or the ISM a retarding drag force F_{drag} is applied. If v is the instantaneous velocity the simplest model which is usually considered is that with

$$F_{drag} \propto v^n \quad , \tag{1}$$

with n as an integer. Here the case of $n = 1$ and $n = 2$ is considered. In classical mechanics $n = 1$ is referred to as Stoke's law of resistance and $n = 2$ as Newton's law of resistance. We now consider two laminar jets and the turbulent case separately.

2.1. *Stoke's behaviour*

Consider a slice of the jet with mass m. The equation of motion is given by

$$m\frac{dv}{dt} = -bv \tag{2}$$

or

$$\frac{dv}{dt} = -Bv \quad , \tag{3}$$

where $B = b/m$. The temporal behaviour of the velocity turns out to be

$$v = v_0 e^{-Bt} \quad , \tag{4}$$

where v_0 is the initial velocity. The distance at the time t is

$$x = \frac{v_0}{B}(1 - e^{-Bt}) \quad , \tag{5}$$

and this can be considered the first law of motion. The velocity space dependence is

$$v - v_0 = -Bx \quad . \tag{6}$$

The velocity of the jet is allowed to vary between a maximum value at the beginning (the inner region), $v = v_0 = \frac{c}{c_f}$ with c_f a number larger than one, and a minimum value at the end (the outer region), for example $v = \frac{c}{10000}$. In this way the coefficient B can be found by identifying x with the jet's length x_1

$$B = \frac{v_0 - c/10000}{x_1} \quad . \tag{7}$$

The lifetime of the radiosource, t_{RS}^{Stoke}, can be derived from equation (4) once the numerical value of B is known

$$t_{RS}^{Stoke} = \frac{ln \frac{v_0 \times 10000}{c}}{B} \quad , \tag{8}$$

that becomes

$$t_{RS}^{Stoke} = \frac{ln \frac{10000}{c_f}}{B} \quad . \tag{9}$$

2.2. *Newton's behaviour*

The equation of motion is now

$$m \frac{dv}{dt} = -av^2 \quad , \tag{10}$$

or

$$\frac{dv}{dt} = -Av^2 \quad , \tag{11}$$

where $A = a/m$. The temporal behaviour of the velocity turns out to be

$$v = \frac{v_0}{1 + v_0 At} \quad , \tag{12}$$

and the distance

$$x = \frac{ln(Av_0t + 1)}{A} \quad , \tag{13}$$

which can be considered the second law of motion. The velocity space dependence is

$$x = \frac{-ln \ \frac{vc_f}{c}}{A} \quad . \tag{14}$$

The coefficient A can be found by inserting $\frac{v}{c} = 1/10000$ which corresponds to $v = 30$ km s^{-1} while L, the length of the jets is equal to x, later called x_1.

Here, the lifetime of the radiosource, t_{RS}^{Newton}, can be derived from equation (12) once the numerical value of A is known

$$t_{RS}^{Newton} = (\frac{c}{c_f v} - 1)\frac{c_f}{cA} \quad . \tag{15}$$

2.2.1. *Parameters of the artificial viscosity from a sample of WAT*

A sample of 7 radio-galaxies classified as Wide Angle Tails (WAT) was imaged sensitively at high resolution by Hardcastle & Sakelliou (2004). This sample is here considered as a source of data that allows us to derive the parameters of Section 2.2 and Section 2.1, see Table 1. The parameters of the first two laws of motion are found once the averaged velocity at the beginning of the jet (alias c_f) and at the end of the jet are fixed by observational arguments. The spectroscopic measurements are a good candidate to find the jet's velocity but attention should be paid to the fact that at a given position x the velocity can vary considerably from the boundary to the center of the jet, see equation (21).

TABLE 1

ARTIFICIAL VISCOSITY PARAMETERS OF SEVEN WAT[1]

Radio name	x_1 [kpc]	$t_{RS}^{Stoke}[10^6\text{year}]$	B[1/year]	$t_{RS}^{Newton}[10^6\text{year}]$	A[1/pc]
0647+693	81	2.9	3.10×10^{-6}	2.8×10^{2}	1.1×10^{-4}
1231+674	35	1.25	7.13×10^{-6}	1.2×10^{2}	2.56×10^{-4}
1333+412	20	0.79	1.24×10^{-5}	71	4.49×10^{-4}
1433+674	49	1.76	5×10^{-6}	1.7×10^{2}	1.83×10^{-4}
2236−176	44	1.58	5.67×10^{-6}	1.5×10^{2}	2.0×10^{-4}
3C465	28	1.0	8.9×10^{-6}	99	3.2×10^{-4}
1610−608	13	0.46	1.8×10^{-5}	46	6.9×10^{-4}

[1] $c_f = 1.25$ and velocity at the end v/c=1/10000. The value of c_f is chosen in order to have relativistic velocities in the initial stage (inner region) of the jet.

2.3. *Turbulent jets*

The theory of turbulent jets emerging from a circular hole can be found in different books with different theories, see Bird, Stewart, & Lightfoot (2002), Landau (1987), and Goldstein (1965). The basic assumptions common to the three already cited approaches are

1. The rate of momentum flow, J, represented by

$$J = const \times \rho b^2 \overline{v}_{x,max}^2 \quad , \tag{16}$$

is constant; here x is the distance from the initial circular hole, $b(x)$ is the jet's diameter at distance x, $\overline{v}_{x,max}$ is the maximum velocity along the the centerline, $const$ is

$$const = 2\pi \int_0^\infty f^2 \xi d\xi \quad , \tag{17}$$

where

$$f(\xi) = \frac{\overline{v}_x}{\overline{v}_{x,max}} \quad \text{with} \quad \xi = \frac{x}{b_{1/2}} \quad , \tag{18}$$

and ρ is the density of the surrounding medium, see equation (5.6-3) in Bird et al. (2002).

2. The jet's density ρ is constant over the expansion and equal to that of the surrounding medium.

When omitting the details of the computation, an expression can be found for the average velocity $\overline{v}_x$, see equation (5.6-21) in Bird et al. (2002),

$$\overline{v}_x = \frac{\nu^{(t)}}{x} \frac{2C_3^2}{\left[1 + \frac{1}{4}(C_3 \frac{r}{x})^2\right]^2} \quad , \tag{19}$$

where $\nu^{(t)}$ is the kinematical eddy viscosity and C_3, see equation (5.6-23) in Bird et al. (2002),

$$C_3 = \sqrt{\frac{3}{16\pi}} \sqrt{\frac{J}{\rho}} \frac{1}{\nu^{(t)}} \quad . \tag{20}$$

An important quantity is the radial position, $r = b_{1/2}$, corresponding to an axial velocity one-half of the centerline value, see equation (5.6-24) in Bird et al. (2002),

$$\frac{\overline{v}_x(b_{1/2}, x)}{\overline{v}_{x,max}(x)} = \frac{1}{2} = \frac{1}{\left[1 + \frac{1}{4}(C_3 \frac{b_{1/2}}{x})^2\right]^2} \quad . \tag{21}$$

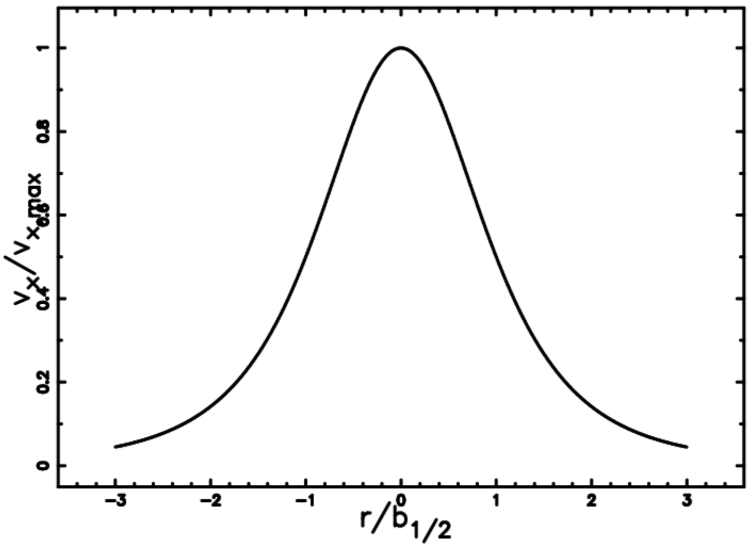

Fig. 1. Mean velocity profile vs. channel radius in a circular jet in turbulent flow. The velocity distribution is a function growing from zero (at the wall of the channel) to a maximum value in the central region.

The experiments in the range of Reynolds number, Re, $10^4 \leq Re \leq 310^6$ (see Reichardt 1942; Reichardt 1951; Schlichting 1979) indicate that

$$b_{1/2} = 0.0848x \quad , \tag{22}$$

and as a consequence

$$C_3 = 15.17 \quad , \tag{23}$$

and therefore

$$\frac{\overline{v}_x(r)}{\overline{v}_{x,max}(r)} = \frac{1}{\left[1 + 0.414\ (r/b_{1/2})^2\right]^2} \quad . \tag{24}$$

Figure 1 reports the behaviour of the velocity distribution as given by equation (24).

The average velocity, $\overline{v}_x$, is $\approx$ 1/100 of the centerline value when $r/b_{1/2} = 4.6$ and this allows us to say that the diameter of the jet is

$$b = 2 \times 4.6 b_{1/2} \quad . \tag{25}$$

On introducing the opening angle α, the following new relationship is found

$$\frac{\alpha}{2} = \arctan \frac{4.6 b_{1/2}}{x} \quad . \tag{26}$$

The generally accepted relationship between the opening angle and Mach number, see equation (A33) in De Young (2002), is

$$\frac{\alpha}{2} = \frac{c_s}{v_j} = \frac{1}{M} \quad , \tag{27}$$

where c_s is the sound velocity, v_j the jet's velocity and M the Mach number. The new relationship (26) replaces the traditional relationship (27). The parameter $b_{1/2}$ can therefore be connected with the jet's geometry

$$b_{1/2} = \frac{1}{4.6} \tan(\frac{\alpha}{2}) x \quad . \tag{28}$$

If this approximate theory is accepted, equation (22) gives $\alpha = 42.61°$: this is the theoretical value that originates the so called Reichardt profiles. The value of $b_{1/2}$ fixes the value of C_3 and therefore the eddy viscosity is

$$\nu^{(t)} = \sqrt{\frac{3}{16\pi}}\sqrt{\frac{J}{\rho}}\frac{1}{C_3} = \sqrt{\frac{3}{16\pi}}\sqrt{const}\, bv_{x,max}\frac{1}{C_3} \quad . \tag{29}$$

In order to continue, the integral that appears in *const* should be evaluated, see equation (17). A numerical integration gives

$$\int_0^\infty f^2 \xi d\xi = 0.402 \quad , \tag{30}$$

and therefore

$$const = 2.528 \quad . \tag{31}$$

On introducing typical parameters of jets like α=5°, $v_{x,max}$=v_{100} = v[km s^{-1}]/100, $b = b_1$ where b_1 is the momentary radius in kpc, it is possible to deduce an astrophysical formula for the kinematical eddy viscosity

$$\nu^{(t)} = 0.0028\, b_1 v_{100}\frac{\mathrm{kpc}^2}{10^7\mathrm{year}} \quad \mathrm{when} \quad C_3 = 135.61 \quad . \tag{32}$$

This paragraph concludes underlining the fact that in extragalactic sources it is possible to observe both a small opening angle, $\approx$ 5°, see Section 7.4, and large opening angles, i.e. $\approx$ 34° in the outer regions of 3C31 Laing & Bridle (2004).

3. A CONTINUOUS MODEL

The jet is now explained as due to a continuous flow in a given direction.

The constrained basic elements of our theory are the mean spread rate of the jet measured on the radio maps, the linear density of energy and the initial jet radius r_i. The turbulent hyper-sonic flow, Mach number > 6, is one of the most complicated problems in fluid mechanics. Here the key assumption is that due to the turbulent mass transfer, the density in the jet is the same as in the surrounding medium, see for example equation (10.25) in Hughes & Brighton (1967). This allows the jet law of motion to be expressed in terms of the IGM's density. We identify our jet with a pyramidal section characterised by a solid angle $\Delta\,\Omega$ and overall length x_1. From a practical point of view, α_0 (the first opening angle) is reported in the captions. The solid angle $d\Omega$ in spherical coordinates (r, θ, ϕ) is

$$d\Omega = \sin(\theta) d\theta d\phi \quad . \tag{33}$$

On shifting to the finite differences, the following is obtained

$$\Delta\Omega = (\cos(0) - \cos(\alpha_0\frac{2\pi}{360}))(\alpha_0\frac{2\pi}{360}) \;\; \mathrm{st} \quad , \tag{34}$$

that when the angles are small becomes

$$\Delta\Omega \approx \frac{1}{2}\left(\frac{\alpha_0 2\pi}{360°}\right)^3 \mathrm{st} \quad , \tag{35}$$

where α_0 represents the limit of the integration and is expressed in degrees.

As an example, when α_0=10°, $\Delta\,\Omega$ = 2.65 10^{-3} st. A plot that depicts the assumed geometry is reported in Figure 2.

The approximate advancing area of the jet of momentary length x, A_j, will therefore be

$$A_j \approx x^2 \Delta\Omega \quad . \tag{36}$$

The jet is divided in many slices perpendicular to the direction of motion, each one of thickness r_i (the initial radius); the number of slices, n_j, is therefore

$$n_j = NINT(\frac{x_1}{r_i}) \quad , \tag{37}$$

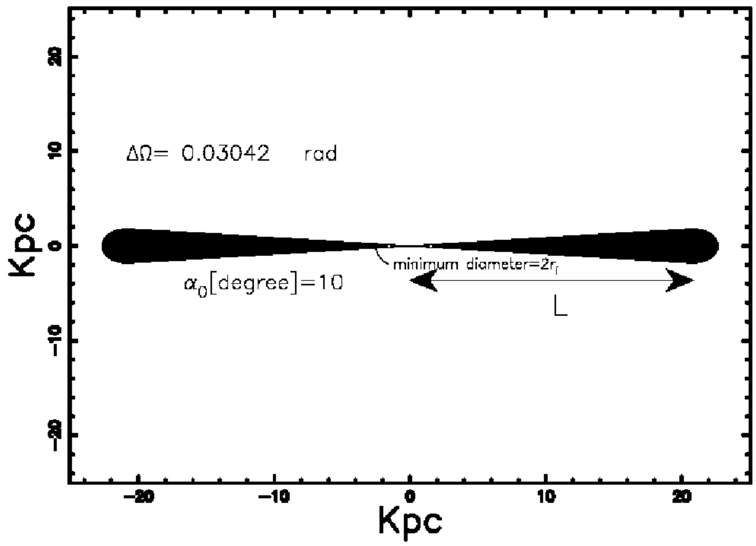

Fig. 2. Two-dimensional view of the continuous jet; the physical parameters are the same as the simulation of NGC4061, see Figure 5.

where NINT denotes the nearest integer. The volume of slice, V_s, is

$$V_s = x^2 \Delta\Omega r_i \quad , \tag{38}$$

and the mass acquired by a slice from the external medium of density ρ is

$$\Delta M = \rho \times V_s = \rho x^2 \Delta\Omega r_i \quad . \tag{39}$$

The hypothesis of a jet in which ρ is constant is used in the theory of turbulent jets, see Section 2.3. The equation that represents momentum conservation is:

$$\frac{d}{dt}\left(\Delta M \dot{x}\right) = p x^2 \Delta\Omega \quad , \tag{40}$$

where p is the pressure. In the case of constant density, equation (40) becomes

$$\frac{d}{dt}\left(x^2 \dot{x}\right) = \frac{p x^2}{\rho r_i} \quad . \tag{41}$$

The pressure of the internal gas decreases according to the adiabatic law

$$p = p_i \left(\frac{V_i}{V}\right)^{5/3} \quad , \tag{42}$$

where V_i is the volume of the first slice and

$$p_i = \frac{2}{3}\frac{E/n_j}{V_i} \quad . \tag{43}$$

Under the adiabatic hypothesis, the differential equation (41) is transformed in

$$\frac{d}{dt}\left(x^2 \dot{x}\right) = H x^{-4/3} \quad , \tag{44}$$

where

$$H = \frac{1}{\rho} p_i \frac{1}{r_i^{-7/3} \Delta\Omega^{5/3}} \quad , \tag{45}$$

and

$$p_i = \frac{2/3\ E}{x_1 r_i^2} \quad . \tag{46}$$

To integrate this equation, $x^2\dot{x} = Ax^\alpha$ is used. After adopting the initial condition of $x = 0$ at $t = 0$ and assuming ρ is constant, the equation representing the third law of motion is obtained

$$x = \left(\frac{13}{18}\frac{(3\alpha+4)}{\alpha}Ht^2\right)^{3/13} \quad , \tag{47}$$

and since $\alpha = 5/6$:

$$x = \left(\frac{507}{90}Ht^2\right)^{3/13} \quad . \tag{48}$$

The velocity of the jet turns out to be:

$$v(t) = \dot{x} = \frac{6}{13}\frac{x}{t} \quad . \tag{49}$$

The astrophysical quantities can now be introduced

$$x(t) = 2.541\,\mathrm{kpc}\left(\frac{{t_7}^2 E_{56}\sqrt[3]{r_i^1}}{x_1^1\ \Delta\Omega^{5/3} n_0}\right)^{3/13} \quad , \tag{50}$$

where $E_{56} = E/10^{56}$ ergs, $r_i^1 = r_i/1$kpc, $x_1^1 = x_1/1$kpc, $t_7 = t/(10^7)$ year and $\rho = n_0\ m_H$ with n_0 representing the number of particles in a cubic centimetre and m_H the hydrogen mass. A similar formula is deduced for the velocity

$$\dot{R} = 114.92\ \mathrm{km\ s^{-1}}\left(\frac{E_{56}\sqrt[3]{r_i^1}}{x_1^1\ \Delta\Omega^{5/3} n_0}\right)^{3/13} t_7^{-7/13} \quad . \tag{51}$$

In the case of SNR a comparison can be made with the radius $R(t) \propto\ t^{2/7}$ of the adiabatic phase of the SNR, see for example McCray (1987), and with $R(t) \propto\ t^{2/5}$ of the so-called Sedov solution, see Sedov (1959) and Landau (1987):

$$R(t) = (\frac{25}{4}\frac{E\,t^2}{\pi\,\rho})^{1/5} \quad , \tag{52}$$

where t represents the time, E is the energy injected in the explosion, and ρ is the density of matter. When the jets are analyzed a comparison can be made with the solution presented in Kaiser & Alexander (1997). In their model the density ρ_x of the gas surrounding the jets scales as

$$\rho_x = \rho_0(\frac{d}{a_0})^{-\beta} \quad , \tag{53}$$

where d is the radial distance from the core of the source, ρ_0 is the initial density, a_0 is the scale length and β a parameter comprised between 0 and 2. Their length of the jet L_j scales as

$$L_j \propto t^{3/5-\beta} \quad , \tag{54}$$

and explains the division between FRI and FRII objects in jet power.

4. TWO–PHASE CONTINUOUS MODEL

The starting point is the conservation of the momentum's flux in a "turbulent jet" as outlined in Landau (1987, p. 147). The initial point is characterised by the following section:

$$A_0 = \pi\ r_0^2 \quad . \tag{55}$$

Once α_0 the first opening angle, x_0 the initial position on the x–axis and v_0 the initial velocity are introduced, section A at position x is

$$A(x) = \pi\big(r_0 + (x - x_0)\tan\big[(1/2)\,\alpha_0\big]\big)^2 \quad . \tag{56}$$

The conservation of the total momentum flux states that

$$\rho v_0^2 A_0 = \rho v(x)^2 A(x) \quad , \tag{57}$$

where $v(x)$ is the velocity at position x. The previous equation is valid if the pressure along the jet is constant and viscosity effects are either not considered or have the same effect on the whole momentum flux along the jet. Due to the turbulent transfer, the density ρ is the same on both sides of equation (57). The trajectory of the jet as a function of time is easily deduced from equation (57)

$$x = -\frac{-x_0\,\tan\big[(1/2)\,\alpha_0\big] + r_0 - \sqrt{r_0\,\left(r_0 + 2\,\tan\big[(1/2)\,\alpha_0\big]\,v_0\,t\right)}}{\tan\big[(1/2)\,\alpha_0\big]} \quad , \tag{58}$$

and this can be considered the fourth law of motion. The velocity turns out to be

$$v(t) = \frac{v_0\,r_0}{\sqrt{r_0\,\left(r_0 + 2\,\tan\big[(1/2)\,\alpha_0\big]\,v_0\,t\right)}} \quad . \tag{59}$$

In the applications of equation (58) and (59) r_0, r, x_0 and x will be expressed in kpc, the time t in units of 10^7 year, v_0 and $v(x)$ in kpc/10^7 year. The velocity v_0 can be parametrised as a function of the velocity of light c as $v_0 = \frac{c}{c_f}$ where c_f is an input parameter allowed to vary between 1.2 and 10.

It is now possible to introduce the two-phase beam in which, due to a certain physical phenomenon, for example the evolution of the K-H instabilities, the beam abruptly increases the opening angle, that from α_0 (first opening angle) becomes α_1 (second opening angle). This phenomenon happens at a given time t_1 ($t_1 < t_2$) and a corresponding length x_1 ($x_1 < x_2$): here t_2 denotes the age of the radio-source and x_2 its global length. In this second phase the trajectory is

$$x = -\frac{-x_1\,\tan\left[(1/2)\,\alpha_1\right] + r_1 - \sqrt{r_1\,\left(r_1 + 2\,\tan\left[(1/2)\,\alpha_1\right]v_1\,(t - t_1)\right)}}{\tan\left[(1/2)\,\alpha_1\right]} \quad , \tag{60}$$

and the velocity

$$v(t) = \frac{v_1\,r_1}{\sqrt{r_1\,\left(r_1 + 2\,\tan\left[(1/2)\,\alpha_1\right]v_1\,(t - t_1)\right)}} \quad . \tag{61}$$

5. TWO–PHASE RELATIVISTIC MODEL

The starting point is the energy momentum tensor, T^{ik},

$$T^{ik} = wu^iu^k - pg^{ik} \quad , \tag{62}$$

where u^i is the 4-velocity, i varies from 0 to 3, w is the enthalpy for unit volume, p is the pressure and g^{ik} the metric of the manifold, see Landau (1987). The condition for momentum conservation in the presence of velocity, v, along one direction states that

$$\left(w(\frac{v}{c})^2\frac{1}{1\,-\,v^2/c^2} + p\right)A = const \quad , \tag{63}$$

where A is the considered area in the direction perpendicular to the motion. The enthalpy per unit volume is

$$w = c^2\rho + p \quad , \tag{64}$$

where ρ is the density, and c the light velocity. The reader may be puzzled by the Γ^2 factor in equation (63), where $\Gamma^2 = \frac{1}{1\,-\,v^2/c^2}$. However it should be remembered that w is not an enthalpy, but an enthalpy per unit volume: the extra Γ factor arises from a "length contraction" in the direction of motion.

With the assumption of turbulent jets, $p = 0$, the momentum conservation law is obtained

$$\left(\rho v^2 \frac{1}{1 - v^2/c^2}\right) A = const \quad . \tag{65}$$

This equation is equal to equation (A.32), the jet "thrust", in De Young (2002). Note the similarity between the previous formula and condition (135.2) in Landau (1987) concerning the shock waves: when A=1 they are equal.

In two sections of the jet we have:

$$\rho\, {v_0}^2 \pi\, {r_0}^2 \, \frac{1}{1 - {v_0}^2/c^2} = \rho\, v^2 \left[\left(\pi\, {r_0}^2 + \pi\, r_0\, x\alpha_0 + O({\alpha_0}^2)\right)\right] \frac{1}{1 - v^2/c^2} \quad , \tag{66}$$

where v is the velocity at position x, v_0 the velocity at x=0, and α_0 the opening angle of the jet. Also here due to the turbulent transfer, the density ρ is the same on both sides of equation (66) and the following second degree equation in $\beta = \frac{v}{c}$ is obtained:

$$\beta^2 r_0 + \beta^2 x\alpha_0 - \beta^2 {\beta_0}^2 x\alpha_0 - {\beta_0}^2 r_0 = 0 \tag{67}$$

where $\beta_0 = \frac{v_0}{c}$. The positive solution is:

$$\beta = \frac{\sqrt{r_0}\beta_0}{\sqrt{r_0 + x\alpha_0 - {\beta_0}^2 x\alpha_0}} \quad . \tag{68}$$

From equation (68) it is possible to deduce the distance $x_{1/2}$ after which the velocity is half of the initial value:

$$x_{1/2} = -3\, \frac{r_0}{\alpha_0 \left(-1 + {\beta_0}^2\right)} \quad . \tag{69}$$

In FR-II's radio-galaxies the velocity is thought to be relativistic until termination at hot-spots; equation (69) states that the typical distance over which the jet is relativistic is a function of the three parameters α_0, r_0 and β_0.

The trajectory of the relativistic jet as a function of the time can be deduced from equation (68) and is

$$\int_0^x \frac{\sqrt{r_0 + x\alpha_0 - {\beta_0}^2 x\alpha_0}}{\sqrt{r_0}\beta_0} dx = ct \quad . \tag{70}$$

On integrating it is possible to obtain the equation of the trajectory

$$2/3\, \frac{{r_0}^{3/2} - \left(r_0 + x\alpha_0 - {\beta_0}^2 x\alpha_0\right)^{3/2}}{\alpha_0 \left(-1 + {\beta_0}^2\right) \sqrt{r_0}\beta_0} - ct = 0 \quad . \tag{71}$$

After some manipulation equation (71) becomes

$$\begin{aligned}
&\left(-3\,{\alpha_0}^3 {\beta_0}^2 + 3\,{\alpha_0}^3 {\beta_0}^4 - {\beta_0}^6 {\alpha_0}^3 + {\alpha_0}^3\right) x^3 + \\
&\left(3\, r_0\, {\alpha_0}^2 - 6\, r_0\, {\alpha_0}^2 {\beta_0}^2 + 3\, r_0\, {\beta_0}^4 {\alpha_0}^2\right) x^2 + \\
&\left(-3\, {r_0}^2 {\beta_0}^2 \alpha_0 + 3\, {r_0}^2 \alpha_0\right) x - \\
&9/4\, c^2 t^2 {\alpha_0}^2 r_0\, {\beta_0}^6 - 3\, {r_0}^2 ct\alpha_0\, \beta_0 + 3\, {r_0}^2 ct\alpha_0\, {\beta_0}^3 - \\
&9/4\, c^2 t^2 {\alpha_0}^2 r_0\, {\beta_0}^2 + 9/2\, c^2 t^2 {\alpha_0}^2 r_0\, {\beta_0}^4 = 0 \quad .
\end{aligned} \tag{72}$$

The parameter p, see Appendix 10.5, that regulates the solutions of the cubic equation is now evaluated. When equation (72) is considered we have $p = 0$ and therefore we have one real root that is (the fifth law of motion):

$$x(t) = -1/2\, \frac{-2\, r_0 + \sqrt[3]{2}\sqrt[3]{r_0}\, \left(2\, r_0 + 3\, ct\alpha_0\, \beta_0 - 3\, ct\alpha_0\, \beta_0^3\right)^{2/3}}{\alpha_0 \left(-1 + {\beta_0}^2\right)} \quad . \tag{73}$$

The velocity of the relativistic jet as function of the time is

$$v(t) = \frac{c\beta_0\ \sqrt[3]{r_0}\ \sqrt[3]{2}}{\sqrt[3]{2\,r_0 + 3\,ct\alpha_0\,\beta_0 - 3\,ct\alpha_0\,\beta_0^3}} \quad . \tag{74}$$

The velocity v_0 can be parametrised as a function of the parameter β_0, a parameter allowed to vary between 0.1 and 0.99999. The two previous equations can be expressed in astrophysical units once $r_0^1 = r_0/1\mathrm{kpc}$ and $t_7 = t/(10^7)$year are introduced

$$x(t) = 1/2\,\frac{2\,r_0^1 - \sqrt[3]{2}\ \sqrt[3]{r_0^1}\left(2\,r_0^1 + 9180.0\,t_7\,\alpha\,\beta_0 - 9180.0\,t_7\,\alpha\,{\beta_0}^3\right)^{2/3}}{\alpha\,\left(-1+{\beta_0}^2\right)}\mathrm{kpc} \quad , \tag{75}$$

and

$$v(t) = 299788.2\,\frac{\beta_0\ \sqrt[3]{r_0^1}\,\sqrt[3]{2}}{\sqrt[3]{2\,r_0^1 + 9180.0\,t_7\,\alpha\,\beta_0 - 9180.0\,t_7\,\alpha\,{\beta_0}^3}}\ \mathrm{km\ s^{-1}} \quad . \tag{76}$$

The transition from relativistic to classical velocity is still represented by equations (60) and (61) but x_1,r_1 and v_1 are the parameters at the end of the relativistic phase.

6. THE CHANGE OF FRAMEWORK

The wide spectrum of observed morphologies that characterises the head-tail radio galaxies could be due to the kinematical effects as given by the composition of the velocities in different kinematical frameworks such as decreasing jet velocity, jet precession, rotation, and proper velocity of the host galaxy in the cluster. These effects were partially analysed in Zaninetti (1989); here part of the developed theory and symbols will be used, and will now be briefly reviewed in order to represent the law of motion through a matrix. Of particular interest is the evaluation of various matrices that will enable us to transform from the inertial coordinate system of the jet to the coordinate system in which the host galaxy is moving in space. The various coordinate systems will be $\mathbf{x}=(x,y,z)$, $\mathbf{x}^{(1)}=(x^{(1)},y^{(1)},z^{(1)})$, $\ldots$ $\mathbf{x}^{(5)}=(x^{(5)},y^{(5)},z^{(5)})$. The vector representing the motion of the jet will be represented by the following 1×3 matrix

$$G = \begin{bmatrix} 0 \\ 0 \\ L(t) \end{bmatrix} \quad , \tag{77}$$

where the jet motion $L(t)$ is considered along the z-axis.

The jet axis, z, is inclined at an angle Ψ_{prec} relative to an axis $z^{(1)}$ and therefore the 3×3 matrix, representing a rotation through the x axis,is given by:

$$F = \begin{bmatrix} 1 & 0 & 0 \\ 0 & \cos(\Psi_{prec}) & \sin(\Psi_{prec}) \\ 0 & -\sin(\Psi_{prec}) & \cos(\Psi_{prec}) \end{bmatrix} \quad . \tag{78}$$

From a practical point of view Ψ_{prec} can be derived by measuring the half-opening angle of the maximum of the sinusoidal oscillations (named wiggles) that characterises the jet.

If the jet is undergoing precession around the $z^{(1)}$ axis, Ω_{prec} can be the angular velocity of precession expressed in radians per unit time; Ω_{prec} is computed from the radio maps by measuring the number of sinusoidal oscillations that characterise the jet. The transformation from the coordinates $\mathbf{x}^{(1)}$ fixed in the frame of the precessing jet to the non-precessing coordinate $\mathbf{x}^{(2)}$ is represented by the 3×3 matrix

$$E = \begin{bmatrix} \cos(\Omega_{prec}\,t) & \sin(\Omega_{prec}\,t) & 0 \\ -\sin(\Omega_{prec}\,t) & \cos(\Omega_{prec}\,t) & 0 \\ 0 & 0 & 1 \end{bmatrix} \quad . \tag{79}$$

The arbitrary orientation of the precession axis relative to the central galaxy at rest, necessitates a transformation from the coordinate frame $\mathbf{x}^{(2)}$ to the frame $\mathbf{x}^{(3)}$. The relative orientations are assumed to be characterised by the Euler angles $(\Phi_j, \Theta_j, \Psi_j)$. There is no uniform agreement on the designation of the Euler angles and the manner in which they are generated. We have chosen here to use the conventions found in Goldstein, Poole, & Safko (2002) and the 3×3 matrix, D_E, is

$$D_E = \begin{bmatrix} cos\Psi_j cos\Phi_j - cos\Theta_j sin\Phi_j sin\Psi_j & cos\Psi_j sin\Phi_j + cos\Theta_j cos\Phi_j sin\Psi_j & sin\Psi_j sin\Theta_j \\ -sin\Psi_j cos\Phi_j - cos\Theta_j sin\Phi_j cos\Psi_j & -sin\Psi_j sin\Phi_j + cos\Theta_j cos\Phi_j cos\Psi_j & cos\Psi_j sin\Theta_j \\ sin\Theta_j sin\Phi_j & -sin\Theta_j cos\Phi_j & cos\Theta_j \end{bmatrix} . \quad (80)$$

On assuming that $\Phi_j = 0°$, $\Psi_j = 0°$ and $\Theta_j = 90°$ we have the simple expression

$$D_E = \begin{bmatrix} 1 & 0 & 0 \\ 0 & 0 & 1 \\ 0 & -1 & 0 \end{bmatrix} . \quad (81)$$

Another 3×3 matrix is introduced which represents the transformation from $(\mathbf{x^3})$ to $(\mathbf{x^4})$ and is defined by a rotation through the axis $z^{(3)}$ of an angle $\Omega_G t$ where Ω_G is the angular velocity of the galaxy expressed in radians/time units; the total angle of rotation of the galaxy being $\alpha = \Omega_G \, t_{max}$:

$$C = \begin{bmatrix} \cos(\Omega_G\, t) & \sin(\Omega_G\, t) & 0 \\ -\sin(\Omega_G\, t) & \cos(\Omega_G\, t) & 0 \\ 0 & 0 & 1 \end{bmatrix} . \quad (82)$$

In the astrophysical applications $\Omega_G = 0$ because the rotation period of a typical elliptical galaxy is less than the lifetime of a typical radio source; only in the case of NGC326 $\Omega_G \neq 0$, see discussion in Section 7.3.

The last translation represents the change of framework from $(\mathbf{x^{(4)}})$, which is co-moving with the host galaxy, to a system $(\mathbf{x^{(5)}})$ in comparison to which the host galaxy is in uniform motion. It should be remembered that the velocity dispersion in the cluster (not to be confused with the recession velocity) is ≈ 600 km s^{-1}, see Table 1 in Venkatesan et al. (1994). The relative motion of the origin of the coordinate system $(x^{(4)}, y^{(4)}, z^{(4)})$ is defined by the Cartesian components of the galactic velocity $\mathbf{v_G}$, and the required 1×3 matrix transformation representing this translation is:

$$B = \begin{bmatrix} v\_x \\ v\_y \\ v\_z\, t \end{bmatrix} . \quad (83)$$

On assuming, for the sake of simplicity, that v_y=0 and v_x=0, the translation matrix becomes:

$$B = \begin{bmatrix} 0 \\ 0 \\ v\_z\, t \end{bmatrix} . \quad (84)$$

In other words, the direction of the galaxy motion in the IGM and the direction of the jet are perpendicular. From a practical point of view the galaxy velocity can be measured by dividing the length of the radio galaxy in a direction perpendicular to the initial jet velocity by the lifetime of the radio source; an example of such measurement is reported in Section 8.2.

TABLE 2

THE DATA FROM THE RADIO MAP OF NGC1265

L_{rad}[ergs/sec]	mean spread rate [degree]
1.1×10^{40}	10

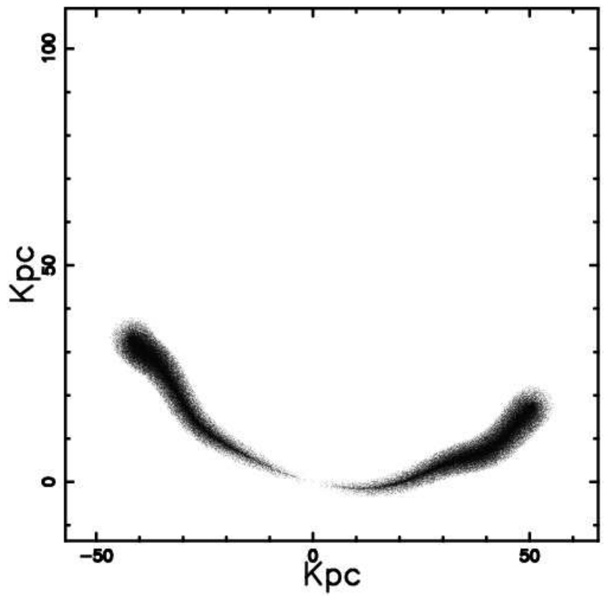

Fig. 3. Continuous three-dimensional trajectory of NGC1265: the three Eulerian angles (English notation) characterising the point of view are Φ=80°, Θ=80° and Ψ=10°. The precession is characterised by the angle Ψ_{prec}=2° and by the angular velocity Ω_{prec}=54.00[°/10^7year]. The three Eulerian angles are: Φ_j=0°, Ψ_j=0° and Θ_j=90°. The angle of rotation of the galaxy is α_G=0°. The physical parameters characterising the jet motion are: E_{56}=0.02, t_1=10.00×10^7year, n_0=0.01 particles/cm^3, x_1=18.00 kpc, r_i=0.90 kpc, α_0=10°.

The final 1×3 matrix A representing the "motion law" can be found by composing the six matrices already described

$$A = B + (C \cdot D_E \cdot E \cdot F \cdot G)$$

$$A = \begin{bmatrix} (\cos(\Omega_G\, t)\sin(\Omega_{prec}\, t)\sin(\Psi_{prec}) + \sin(\Omega_G\, t)\cos(\Psi_{prec}))\, L(t) \\ (-\sin(\Omega_G\, t)\sin(\Omega_{prec}\, t)\sin(\Psi_{prec}) + \cos(\Omega\, galaxy\, t)\cos(\Psi_{prec}))\, L(t) \\ v\_z\, t - \sin(\Psi_{prec})\cos(\Omega_{prec}\, t)\, L(t) \end{bmatrix} . \quad (85)$$

The three components of the previous 1×3 matrix A represent the jet motion along the Cartesian coordinates as given by the observer that sees the galaxy moving in uniform motion.

7. APPLICATION OF THE CONTINUOUS MODEL

The continuous beam model developed in Section 3 is basically represented by equations (50) and (51) and can be easily implemented in a code; this is now applied to various radio–sources.

An attempt to reproduce the mechanical power dependence in the jet trajectory is carried out in Section 7.5.

TABLE 3

THE PHYSICAL PARAMETERS AS OUTPUT OF THE SIMULATION ON NGC1265

x_1 [kpc]	v_z [km s^{-1}]	Δz [kpc]
18.7	84.55	10.3

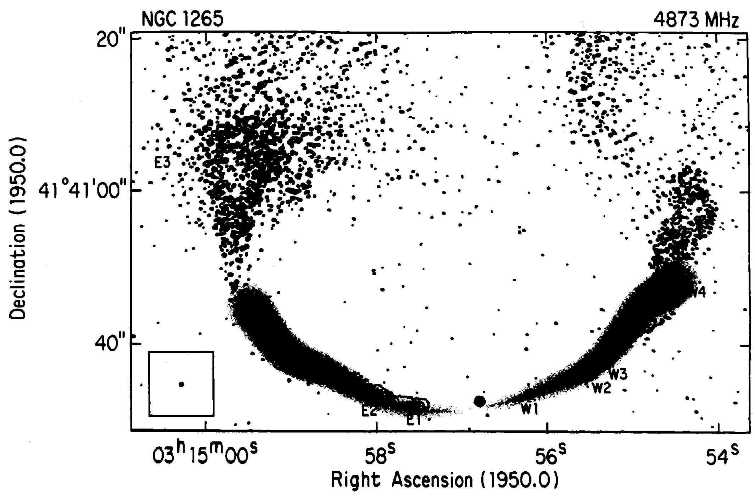

Fig. 4. Figure 1 of Odea & Owen (1986) representing NGC1265 at 4873 MHz superimposed on the theoretical trajectory represented by Figure 3.

TABLE 4

THE DATA FROM THE RADIO MAP OF NGC4061

L_{rad}[ergs/sec]	mean spread rate [degree]
0.06×10^{40}	10

7.1. *The first part of NGC1265*

The first target chosen for our simulation was the radio source NGC1265 at 6 cm. Some basic input parameters extracted from Odea & Owen (1986) are reported in Table 2.

The result of the simulation is reported in Figure 3 and in Figure 4 with the radio map superimposed on the simulation; the adopted input parameters are given in the caption.

The output data as obtained from the code concerning the overall jet length, the perpendicular-displacement, and the galaxy velocity of NGC1265 are reported in Table 3.

7.2. *The first part of NGC4061*

We have chosen the radio source NGC4061 at 21 cm, see Figure 5b in Venkatesan et al. (1994) for a radio map; the basic data as extracted from the radio observations are reported in Table 4. The result of the simulation is visualised in Figure 5 and in Figure 6 with the radio map superimposed on the simulation; the caption of the Figure shows the adopted input parameters while the output data are reported in Table 5.

In this case we know that the velocity dispersion in the cluster is 485 km s^{-1}, see Table 1 in Venkatesan et al. (1994).

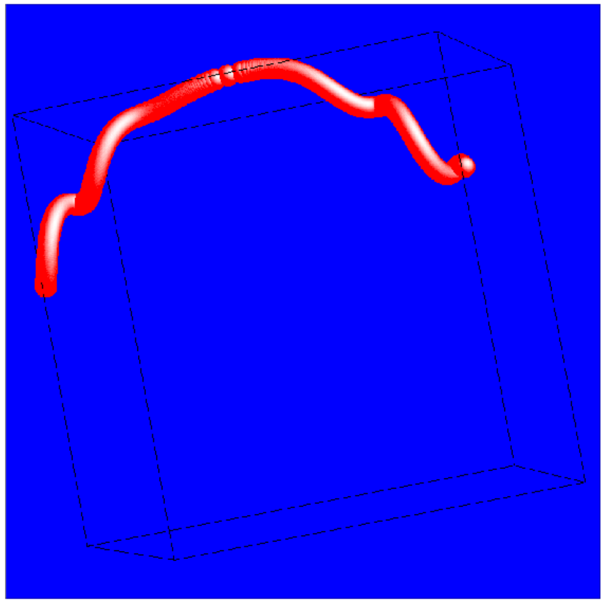

Fig. 5. Continuous three-dimensional trajectory of NGC4061: the three Eulerian angles (English notation) characterising the point of view are Φ=100°, $\Theta = -85°$ and $\Psi = -10°$. The precession is characterised by the angle $\Psi_{prec} = 5°$ and by the angular velocity $\Omega_{prec} = 60.00[°/10^7\text{year}]$. The three Eulerian angles are: Φ_j=0°,Ψ_j=0° and Θ_j=90°. The angle of rotation of the galaxy is α_G=0°. The physical parameters characterising the jet motion are: E_{56}=0.02, t_1=12.00×10^7year, n_0=0.01 particles/cm^3, x_1=20.00 kpc, r_i=1.00 kpc, α_0=10°.

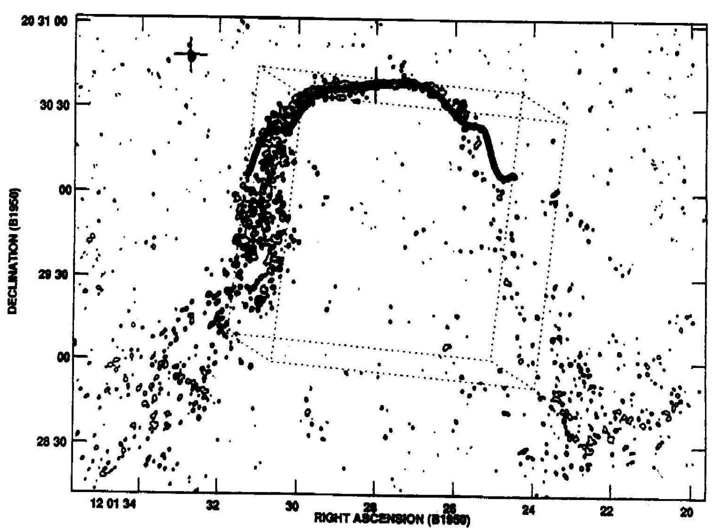

Fig. 6. Figure 5b of Venkatesan et al. (1994) representing NGC4061 at 21 cm superimposed on the theoretical trajectory represented by Figure 5.

The velocity v_z in our model is 119.08 km s^{-1} implying an angle of $\approx$ 14.2° between the direction of the galaxy motion and the initial direction of the jet. A typical plot of the jet velocity as a function of the time is reported in Figure 7.

TABLE 5

THE PHYSICAL PARAMETERS OUTPUT OF THE SIMULATION ON NGC4061

x_1 [kpc]	v_z [km s^{-1}]	Δz [kpc]
20.9	78.65	14.6

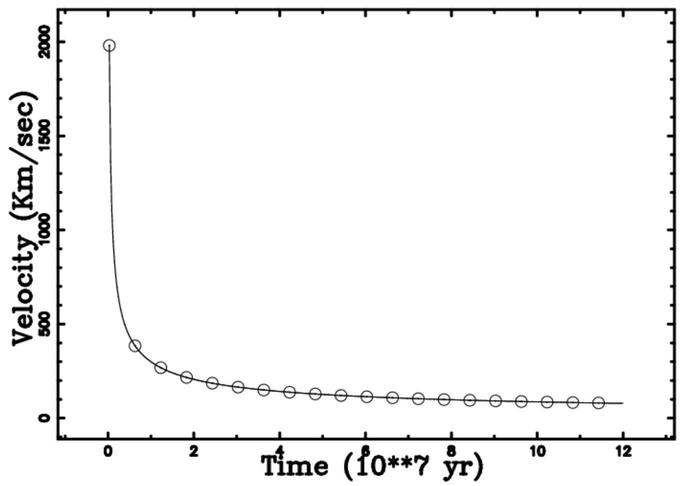

Fig. 7. The numerical relationship between velocity and t_1 in NGC4061. Parameters as in Figure 5.

7.3. *The first part of NGC326*

Another test of our code is the radio galaxy NGC326; in particular we refer to the image at 1.4GHz as given in Figure 6 (bottom panel) of Murgia et al. (2001): the basic input data as deduced from the radio map are reported in Table 6.

In this case, the optical observations with HST reveal two cores, one coincident with the origin of the radio galaxy, and the other at the projected distance of 4.8 kpc. In this case, it is assumed that the rotation of the host galaxy is due to gravitational interaction, the total angle of rotation being α_G=90°. Figure 8 reports on the obtained simulation and Figure 9 reports the radio map superimposed on the simulation; Table 7 gives the output data from the simulation.

7.4. *A sample of WAT*

A sample of 7 radio–galaxies has already been presented in Section 2.2.1 and is now considered as a test of the theory developed in Section 3. A first look at the radio–maps shows a nearly constant opening angle of $\approx$ 5°. On assuming that a constant ratio $E/x_1 = E_{56}/1\text{kpc} = 10^{-3}$ characterises the motion, the terminal velocity v_1 and the age of the jets, t_1, see Table 8, can easily be found through an iterative procedure; the length of the jet being provided in Table 7 of Hardcastle & Sakelliou (2004). From Table 8 the terminal velocities can be compared with the central galaxy velocity dispersion in the cluster.

Most of the jets here considered are distinctly one sided over the length modelled, and this fact is here justified by the flip-flop mechanism rather than assuming that they are relativistic over the whole length.

7.5. *Power transition*

The morphological transition between FR–I and FR–II objects can be explained under the assumption of constant power P, i.e. negligible synchrotron losses. Equation (50) can be modified by inserting the total power

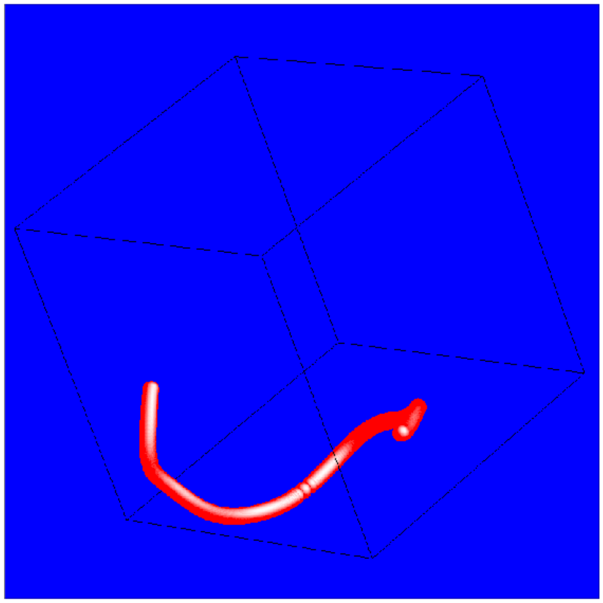

Fig. 8. Continuous three-dimensional trajectory of NGC326: the three Eulerian angles (English notation) characterising the point of view are Φ=110°, Θ=65° and Ψ=-40°. The precession is characterised by the angle Ψ_{prec}=2° and by the angular velocity Ω_{prec}= 51.43 [°/10^7year]. The three Eulerian angles are: Φ_j=0°, Ψ_j=0° and Θ_j=90°. The angle of rotation of the galaxy is α_G=-90°. The physical parameters characterising the jet motion are: E_{56}=0.03, t_1=14.00×10^7 year, n_0=0.01 particles/cm^3, x_1=30.00 kpc, r_i=1.50 kpc, $\alpha_0 = 6°$.

TABLE 6

THE DATA FROM THE RADIO MAP OF NGC326

L_{rad}[ergs/sec]	mean spread rate [degree]
0.5×10^{40}	6.45

$P = E/t$ and typical parameters of the jet previously adopted such as $\alpha_0 = 5°$ and n_0= 0.001 particles/cm^3:

$$x(t_7) = 36.78\,\mathrm{kpc}\left(\frac{{t_7}^3 P_{33}\,\sqrt[3]{r_i}}{L_1}\right)^{3/13} \quad , \tag{86}$$

where $P_{33} = P/10^{33}\ Watt$. Only the velocity of the host galaxy in the direction perpendicular to that of the jet is here considered

$$y(t_7) = 4.05\mathrm{kpc}\ t_7\ v_{400} \quad , \tag{87}$$

where $v_{400} = v[\mathrm{km\ s}^{-1}]/400$. When a comparison of equation (86) and (87) is made, it is clear that an increase in the mechanical power of the galaxy corresponds to an increase in the elongation along x of the phenomena. A typical plot that tentatively reproduces the power transition is reported in Figure 10.

There are many 'straight' FR-I's, NGC315 is a good example. This can happen when the galaxy's velocity is lower than the standard value here adopted of 400 km s^{-1} or from a particular point of view of the observer.

8. APPLICATION OF THE TWO–PHASE BEAM

The two-phase beam developed in Sections 4 and 5 is now applied to two radio-sources: in one, Cygnus A, the relativistic-classic transition is applied and in the other, 0647+693, the classic-classic transition.

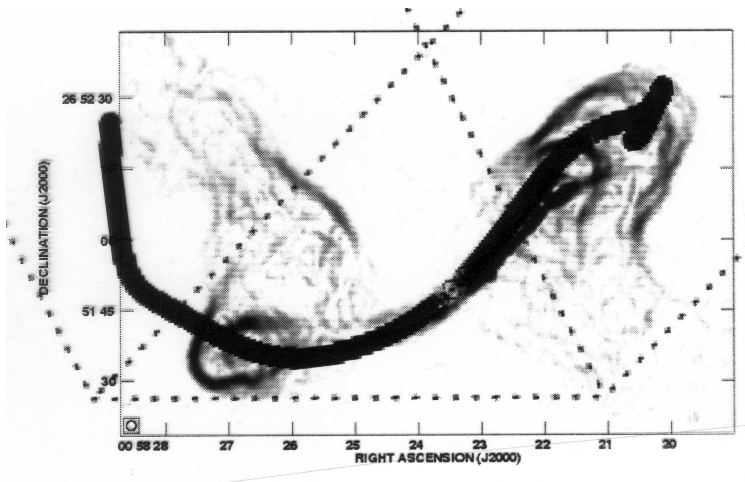

Fig. 9. Figure 6 (bottom panel) of Murgia et al. (2001) superimposed on the theoretical trajectory represented by Figure 8.

TABLE 7

THE PHYSICAL PARAMETERS OUTPUT OF THE SIMULATION ON NGC326

x_1 [kpc]	v_z [km s^{-1}]	Δz [kpc]
30.6	98.71	16.8

8.1. *Relativistic Cygnus A*

A good introduction to the classical double radio sources, as well as to Cygnus A, can be found in chapter 6 of De Young (2002). The main physical parameters characterising the jet in Cygnus A, as presented in Perley, Dreher, & Cowan (1984b), are summarised in Table 9; here x_1^{obs} is the distance between nucleus and hot-spots, α_0^{obs} is the first opening angle (measured on the radio map) and t_{age}^{obs}, the age of the radio–galaxy, as deduced on the basis of the spectral steepening of the lobe emission.

Once the $t_2 = t_{age}^{obs}$ is inserted in the code, the other input parameters are varied in order to obtain $x_1 \approx x_1^{obs}$; this is obtained by solving numerically the integral equation (73). The results of the simulation (as outlined in Section 5) are reported in Figure 11 and in Figure 12 with the radio map superimposed on the simulation; Table 10 reports the data.

8.2. *Classic 0647+693*

A radio–map of 0647+693 in the 8.5 GHz band can be found in Hardcastle & Sakelliou (2004) where two radio-images were traced at the resolution of 0.3×0.6 arcsec and 2 arcsec. The influence of the motion of the host galaxy is evident from the maps and can be visualised in the following way:

- A line is traced between the two hot-spots.
- The perpendicular to the previous line that intersects the nucleus is traced. The distance along the perpendicular to the previous line turns out to be ≈ 36.8 kpc.

From Figure 1 of Hardcastle & Sakelliou (2004) it is also possible to measure the second opening angle, α_1 that turns out to be $\approx 25°$.

The results of the simulation (as outlined in Section 4) are reported in Figure 13 (red points) and in Figure 14, with the radio map superimposed on the simulation; Table 11 reports the data.

TABLE 8

THE SEVEN WAT[1]

Radio name	x_1 [kpc]	v_1 [km s^{-1}]	t_1 [10^7year]
0647+693	81	113	32
1231+674	35	263	6.0
1333+412	20	461	1.95
1433+674	49	188	11
2236−176	44	209	9.5
3C465	28	329	3.8
1610−608	13	708	0.82

[1] $\alpha_0 = 5°$, r_i [kpc] = x_1 [kpc]/100, $n_0 = 10^{-3}$ particles/cm^3 and $E_{56}/1$ kpc = 10^{-3}.

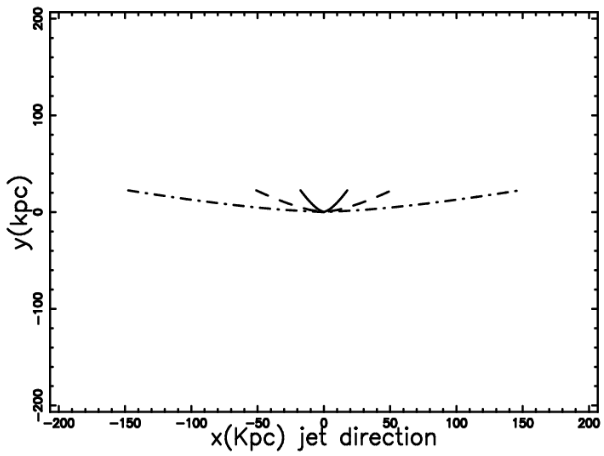

Fig. 10. Three jet trajectories as a function of the power. P_{33}=100 (dot-dash line), P_{33}=1 (dashed line) and P_{33}=0.01 (solid line). The other parameters in common to the three trajectories are $\alpha_0 = 5°$, n_0=0.001 particles/cm^3, L_1=60, r_i=L_1/20, t_7=5.0 and v_{400}=1. The three Eulerian angles are: Φ_j=0°, Ψ_j=0° and Θ_j=90°. The three Eulerian angles (English notation) characterising the point of view are Φ=90°, Θ=90° and Ψ=0°.

In order to reproduce the long trails of 0647+693 visible in Figure 1 of Hardcastle & Sakelliou (2004), the simulation is now performed at a value of t_1 which is larger by factor of four with respect to the previous run, see Figure 13 (green points) and Figure 15, where the radio map is superimposed on the simulation.

9. THE KELVIN-HELMHOLTZ INSTABILITIES

The very small opening angles of observed extra-galactic radio–jets, if interpreted as free expansion, in many cases imply a Mach number $M > 6$ and existing theories are briefly reviewed. Some basic questions can be posed on the stability of such highly supersonic jets:

- Is the jet unstable against perturbations with a wavelength smaller than the radius?
- Is the jet stable over long distances?
- If the jet is unstable, how does the distance over which an instability grows by a factor of e depend upon M and the density contrast between the jet and the external medium?

TABLE 9

THE OBSERVED DATA ON CYGNUS A

x_1^{obs} [kpc]	α_0^{obs} [°]	t_{age}^{obs} [10^7year]
60	5	0.6

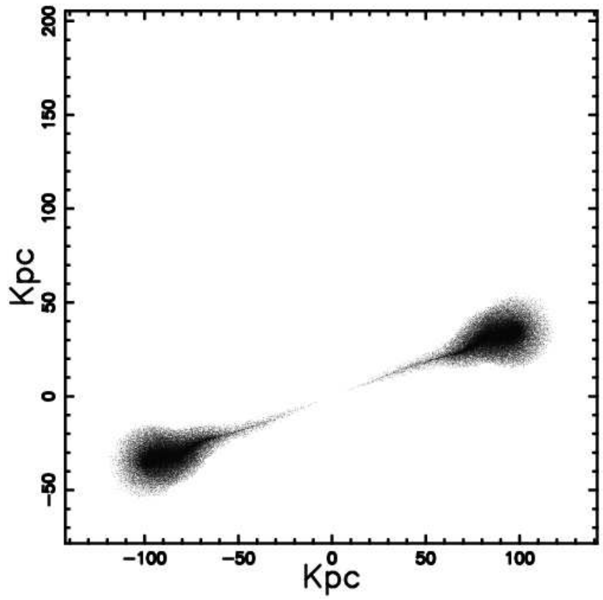

Fig. 11. Projected 3D trajectory of Cygnus A: the three Eulerian angles (English notation) characterising the point of view are Φ=90°, Θ=0° and Ψ=-20°. The precession is characterised by the angle Ψ_{prec}=1° and by the angular velocity Ω_{prec}=600.00 [°/10^7 year]. The three Eulerian angles are: Φ_j=0°, Ψ_j=0° and Θ_j=90°. Parameters of the two-phase continuous model: x_0=0.0 kpc, r_0=0.02 kpc, β_0=0.8, t_2=0.6×10^7 year, t_1= 0.161×10^7 year, α_0=5° and α_1=35°.

- Are the helical instabilities with an azimuthal number m=1 and the pinch instabilities, m=0, enough to build a theory on the lateral growth of the jet due to an increase of energy in the perturbations?

In order to study these questions, we must analyse the Kelvin-Helmholtz instability of an axisymmetric flow along the z-axis when the wavelengths $\lambda = \frac{2\pi}{k}$ (k is the wave-vector) are smaller or greater than the jet radius a, which is taken to be independent of the position along the jet. The velocity, U_0, is assumed to be rectangular. The internal (external) fluid density is represented by ρ_{0i} (ρ_{0e}), the internal sound velocity is s and ν_0= $\frac{\rho_{0i}}{\rho_{0e}}$. The analysis is therefore split in two parts.

9.1. *Small wavelengths*

If the growth rate of the envelope of the reflecting modes is analysed, it is possible to deduce the following approximate relationship for the imaginary (γ_{KH}) and real (ω_r) part of the perturbations when $M > 1$

$$\gamma_{KH} = \gamma_{ad}\frac{s}{a} \tag{88}$$

with

$$\gamma_{ad} \approx 0.17(\ln(kaM))^{1.21}(\frac{2}{\nu_0 + 1/\nu_0})^{0.06}(ka)^{0.7} \quad , \tag{89}$$

and

$$\omega_r \approx \frac{M}{2}\nu_0^{0.21}ka\frac{s}{a} \quad . \tag{90}$$

More details can be found in Zaninetti (1986).

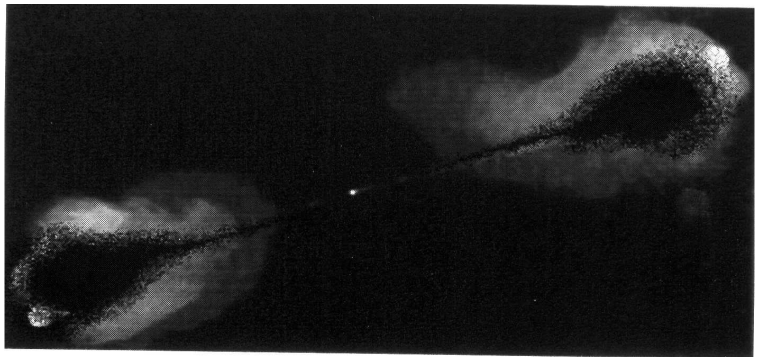

Fig. 12. Cygnus from the NRAO Image Gallery (white) superimposed on the theoretical trajectory represented by Figure 11 (black).

TABLE 10

THE PHYSICAL PARAMETERS OUTPUT OF THE SIMULATION ON CYGNUS A

Physical quantity\index	0	1	2
x [kpc],distance	0.0	60.01	106.18
r [kpc],radius	0.02	5.25	19.81
v [km s^{-1}],velocity	240000	24577	6518
t [10^7year],time	0	0.161	0.6

9.2. *Large wavelengths*

Starting from the equations of motion and continuity, and assuming both fluids to be adiabatically compressible, it is possible to derive and to solve the dispersion relation numerically, see Zaninetti (1987).

We then start from observable quantities that can be measured on radio-maps such as the total length L_{obs}, the wavelength λ^1_{obs} of the wiggles (m=1) along the jet, the distance λ^0_{obs} (m=0) between knots, and the final offset $\Delta\, L_{obs}$ of the center of the jet.

These observable quantities are identified with the following theoretical variables:

$$\lambda^1_{max} = \lambda^1_{obs} \quad , \tag{91}$$

$$\lambda^0_{max} = \lambda^0_{obs} \quad , \tag{92}$$

$$A_0 \exp(\frac{2L_{obs}}{Mt_{ad}a}) = \Delta L_{obs} \quad , \tag{93}$$

$$nl_e = L_{obs} \quad , \tag{94}$$

where $t_{ad} = t_{min} \cdot s_i/a$ and A_0 is the amplitude of the perturbed energy. The result is a theoretical expression for t_{min}, the minimum time scale of the instability, λ_{max}, the wavelength connected with the most unstable mode and l_e, the distance over which the most unstable mode grows by a factor e, see Zaninetti (1987). These parameters can then be found through the set of nonlinear equations previously reported. By choosing three objects, M87 (Owen, Hardee, & Bignell 1980), NGC6251 (see Perley, Bridle, & Willis 1984) and NGC1265 (see Odea & Owen 1986) the observational parameters can be measured on the radio image, see Table 12.

The four nonlinear equations are then solved and the four theoretical parameters are found, see Table 13.

An application of the results here obtained is reported in Figure 16 where the wavelength of the pinch modes (m = 0) and the oscillations of the helical mode (m = 1) as reported in Table 13 are simulated by identifying the lateral growth of energy with the precession. Figure 17 reports the radio map superimposed on the simulation of the pinch modes.

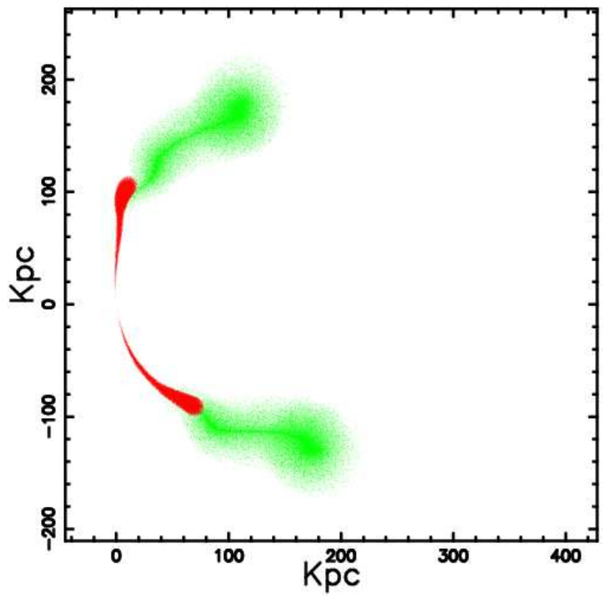

Fig. 13. Projected 3D trajectory of 0647+693 (red points): the three Eulerian angles (English notation) characterising the point of view are Φ=10°, Θ=80° and Ψ=-10°. The precession is characterised by the angle Ψ_{prec}=5° and by the angular velocity Ω_{prec}= 22.50 [°/10^7 year]. The three Eulerian angles are: Φ_j = 0°, Ψ_j = 0° and $Theta_j$=90°. Parameters of the two–phase continuous model: x_0=0.0001 kpc, r_0=0.0600 kpc, c_f=5.0, t_2=8.00×10^7 year, t_1= 4.00×10^7 year, α_0 = 5° and α_1 = 25°. The green points represents the same trajectory after t_2=32.00×10^7 year.

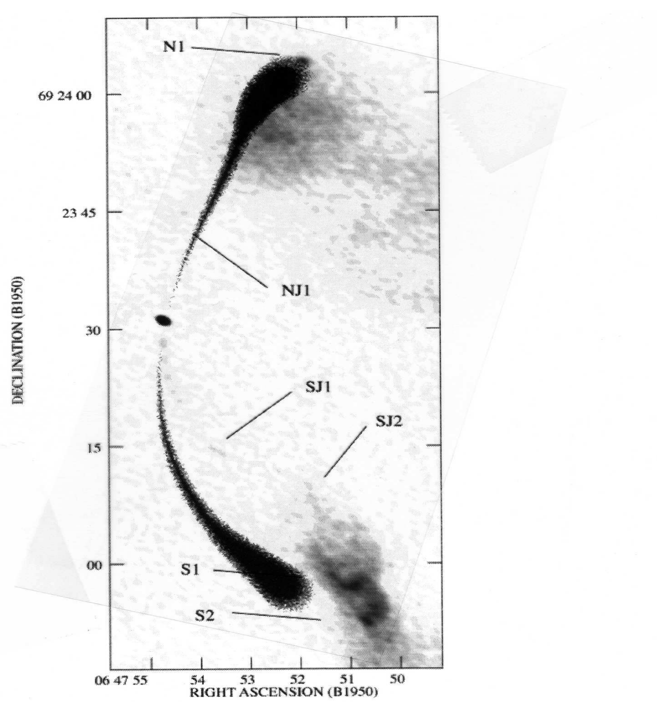

Fig. 14. Figure 2 of Hardcastle & Sakelliou (2004) superimposed on the theoretical trajectory represented by Figure 13 (red points).

TABLE 11

THE PHYSICAL PARAMETERS OUTPUT OF THE SIMULATION ON 0647+693

Physical quantity\position	0	1	2
x [kpc],distance	0.0001	80.7	104.4
r [kpc],radius	0.060	3.6	8.8
v [km s^{-1}],velocity	60000.0	1004.7	407.6
t [10^7 year],time	0	4.0	8.0

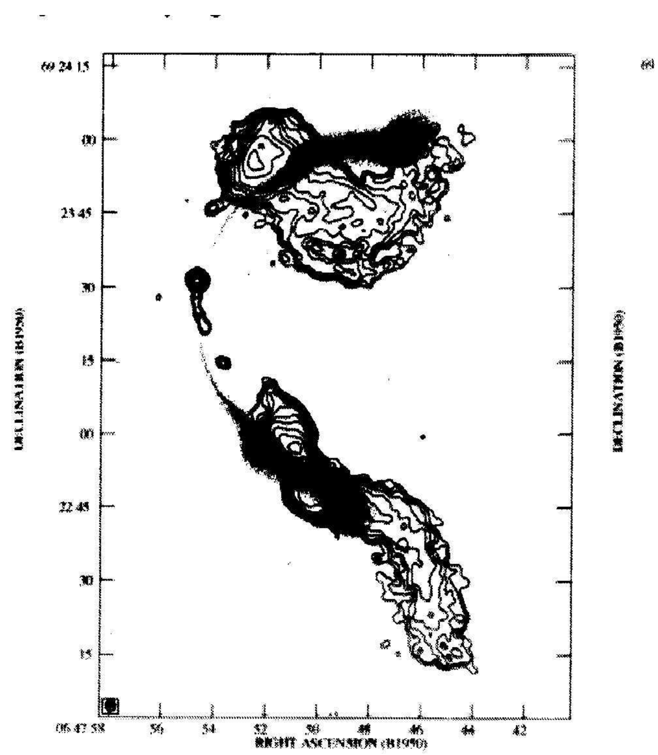

Fig. 15. Figure 1 of Hardcastle & Sakelliou (2004) superimposed on the theoretical trajectory represented by Figure 13 (green points).

10. SUMMARY

10.1. *New Physics*

The concept of deceleration is both an explanation of observed properties of a sample of radio-galaxies, see Laing et al. (1999), as well as a working hypothesis to explain the deceleration of a relativistic jet of electrons and positron pairs by mass injection, see Laing & Bridle (2002b), or by adiabatic models that require coupling between the variations of velocity, magnetic field and particle density, see Laing & Bridle (2002b).

Here two new laws of motion for extra-galactic jets in the presence of laminar flow are derived, equation (5) and equation (13), once the two canonical laws of resistance are introduced.

The introduction of momentum conservation along a solid angle that characterises the extra-galactic jet allows us to find:

- An analytical law, equation (47), for the velocity and length of the jet as a function of the other structural

TABLE 12

PARAMETERS OF THE OBSERVED OSCILLATIONS IN RADIO–GALAXIES EXPRESSED IN AVERAGED RADIUS UNITS

Geometrical misuration	M87	NGC6251	NGC1265
L_{obs} [averaged radius units]	48	58.75	20
λ^0_{obs}[averaged radius units]	4.0	4.89	4
λ^1_{obs}[averaged radius units]	19.2	17.5	13.3
ΔL_{obs} [averaged radius units]	0.96	5.87	2

TABLE 13

THEORETICAL PARAMETERS FROM OSCILLATIONS DEDUCED FROM THE FOUR NONLINEAR EQUATIONS

Theoretical variable	M87	NGC6251	NGC1265
n	2.75	2.88	1.1
M	17.28	19.44	17.93
ν_0	9.61	28.05	9.4
A_0	5.57 10^{-3}	8.2 10^{-3}	0.25

parameters, which are: the involved linear density of energy, the initial radius, the elapsed time and the solid angle. This is the third law of motion.

- An analytical law for the velocity if conversely the conservation of the momentum flux in a turbulent jet is assumed, equation (58). This is the fourth law of motion.
- An integral equation (73) of motion if the conservation of the relativistic momentum flux in a turbulent jet is assumed. This is the fifth law of motion.

The new equation (20) connects the turbulent eddy viscosity with the jet's opening angle.

10.2. *Morphological Results*

The introduction of the law of motion allows us to find a space trajectory on introducing the jet precession, the velocity and rotation of the galaxy, and the inclination of the jet with respect to the plane of the galaxy.

It can therefore be suggested that the hydrodynamical effects necessary to bend the jet (see for example Section 4.4.5 of De Young 2002, or the discussion in Odea 1985) can also be explained as an artifact of a change in the system of reference combined with precession effects of the jet, as well as decreasing jet velocity. From an observational point of view it is not easy to discriminate between the bending of the radio-galaxy due to the dynamic pressure, see equation (A35) in De Young (2002) and the bending due to the decreasing jet velocity. Both models require a virial speed of the host galaxy $\approx$ 1000 km s^{-1} and differ only in the requirement for the jet velocity which is constant in the traditional approach and variable in the models here adopted. This dilemma will be solved when measurements of the jet velocity independent from the radio-models become available. The spectroscopic observations for radio galaxies having ultra steep radio spectra, for example, show velocity shifts ranging from 100 to almost 1000 km s^{-1}, see Roettgering et al. (1997).

10.3. *Other approaches*

In FR-I jets, which are thought to decelerate, the profile of this deceleration appears in other models that are now briefly reviewed:

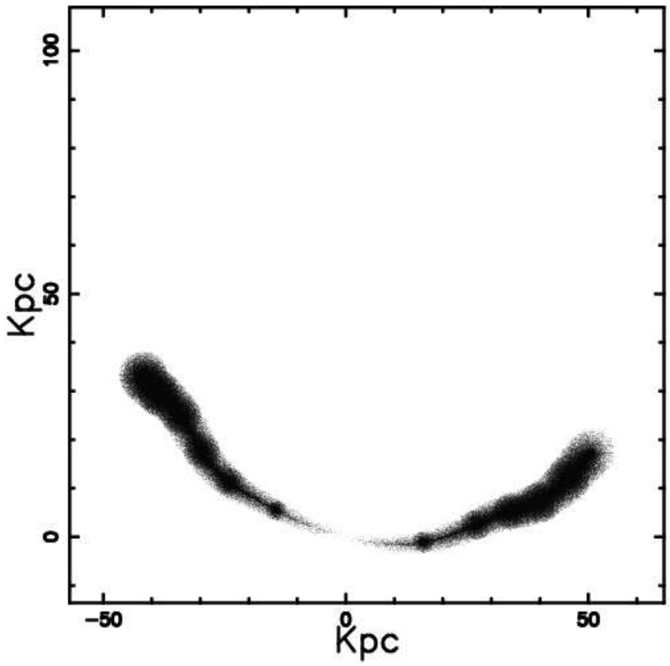

Fig. 16. Parameters as in Figure 3, but with superimposition of the pinch mode ($m = 0$).

- In Bowman, Leahy, & Komissarov (1996) a detailed study of the dynamical effects of entraining cool (thermally sub-relativistic) material into hot (thermally relativistic) jets is presented. The dissipation associated with entrainment causes only a modest loss of kinetic energy flux, and it is shown that relativistic jets are affected much less by dissipation than are classical flows. Their equation (41) represents the flux of kinetic energy, but no analytical results are given for the relativistic law of motion such as our equation (73).

- In Laing & Bridle (2002a) the conservation of particles, energy and momentum is applied in order to derive the variations of pressure and density along the jets of the low-luminosity radio galaxy 3C 31. Their self-consistent solutions for deceleration by injection of thermal matter can be compared with our equation (47).

- In Canvin & Laing (2004) some functional forms are introduced to describe the geometry, velocity, emissivity and magnetic-field structure of the two low-luminosity radio galaxies B2 0326+39 and B2 1553+24 and an accurate comparison between models and data is presented. Their solutions are purely numerical and analytical solutions such as our formula (73) are absent.

10.4. *Analytical results and hydrodynamical codes*

A comparison with the hydrodynamical codes is tentatively made on the following key-points:

- The hydrodynamical codes are usually performed with a family of parameters given by M_b, which is the beam Mach number, while ρ_b is the inside/outside density contrast and t is the time over which the phenomenon is followed. Due to the fact that the hydrodynamical codes do not give the possibility of closing the equations with parameters deduced from the observations, many figures should be produced in order to find the one that better approximates the radiosource chosen to be simulated, see for example Norman (1996) and Balsara & Norman (1992). Conversely, the analytical approach developed here, see equations (5), (13), (50) and (51), gives position and velocity once a few input parameters are provided.

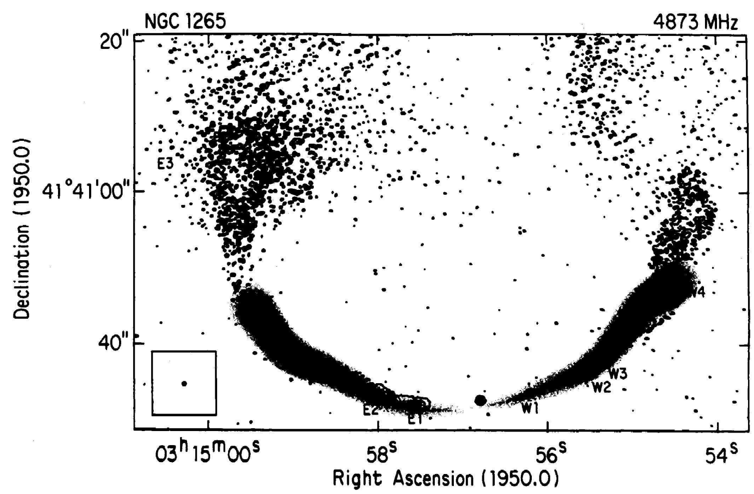

Fig. 17. Figure 1 of Odea & Owen (1986) representing NG1265 at 4873 MHz superimposed on the pinch mode represented by Figure 16.

- The treatment here adopted cannot follow the nonlinear development of the K-H instabilities in 3D, see for example Hardee, Clarke, & Howell (1995) where the simulation was performed at M_b=5; but despite this inconvenience, the concept of developed turbulence with its consequent constant density along the jet is widely used, see Section 3 and Section 4.

10.5. *Average density*

Here we have assumed that the density of the jet is constant and equal to its surrounding medium. This is certainly something that is not necessarily the case for many astrophysical jets. Some properties can be deduced about the medium surrounding the elliptical galaxies from the X-ray surface brightness distribution. Assuming that the gas is isothermal, the following empirical law (Fabbiano 1989) is used for the electron density:

$$n_e(r) = n_e(0)\left[1 + (\frac{r}{ax})^2\right]^{-3\beta/2} \quad , \tag{95}$$

here $\beta \sim 0.4 - 0.6$, $n_e(0) \sim 0.1$ cm^{-3} and $ax \sim 1 - 3$ kpc. On adopting this radial dependence for proton density we can evaluate the average density when $n_e(0) = 0.1$ cm^{-3}, $ax = 2.0$ kpc and $\beta = 0.4$. The average value of n_0, $\overline{n_0}$, when evaluated over 10000 points in the interval 0-100 kpc is $\overline{n_0} = 6.74\ 10^{-3}$ cm^{-3}. This is the theoretical value of n_0 that should be used, for example, in equation (50).

APPENDIX A

The roots of a cubic

To solve the cubic polynomial equation

$$a_0x^3 + a_1x^2 + a_2x + a_3 = 0 \quad , \tag{96}$$

for x, the first step is to apply the transformation

$$x = y - 1/3\,\frac{a_1}{a_0} \quad . \tag{97}$$

This reduces the equation to

$$y^3 + py + q = 0 \quad , \tag{98}$$

where

$$
\begin{aligned}
p &= \frac{1}{3}\,\frac{3\,a_2a_0 - {a_1}^2}{{a_0}^2} \\
q &= \frac{1}{27}\,\frac{27\,a_3{a_0}^2 + 2\,{a_1}^3 - 9\,a_2a_1a_0}{{a_0}^3} \quad .
\end{aligned}
$$

The next step is to compute the first derivative of the left hand side of equation (98) calling it $f(y)'$

$$
f(y)' = 3y^2 + p \quad . \tag{99}
$$

In the case in which $p \geq 0$, in the range of existence $-\infty < y < \infty$, the first derivative is always positive and equation (98) has only one root that is real, more precisely,

$$
y = 1/6\,\sqrt[3]{-108\,q + 12\,\sqrt{12\,p^3 + 81\,q^2}} - 2\,\frac{p}{\sqrt[3]{-108\,q + 12\,\sqrt{12\,p^3 + 81\,q^2}}} \quad , \tag{100}
$$

or equation (96) has the solution in terms of a_0,a_1,a_2 and a_3

$$
\begin{aligned}
&1/6\,\sqrt[3]{-36\,\frac{3\,a_2a_0 - {a_1}^2}{{a_0}^2} + 12\,\sqrt{4/9\,\frac{(3\,a_2a_0 - {a_1}^2)^3}{{a_0}^6} + 9\,\frac{(3\,a_2a_0 - {a_1}^2)^2}{{a_0}^4}}} \\
&-2/3\,\left(3\,a_2a_0 - {a_1}^2\right){a_0}^{-2}\frac{1}{\sqrt[3]{-36\,\frac{3\,a_2a_0 - {a_1}^2}{{a_0}^2} + 12\,\sqrt{4/9\,\frac{(3\,a_2a_0 - {a_1}^2)^3}{{a_0}^6} + 9\,\frac{(3\,a_2a_0 - {a_1}^2)^2}{{a_0}^4}}}} \quad . \qquad (101)
\end{aligned}
$$

(102)

REFERENCES

Alexander, P. 2000, MNRAS, 319, 8
Balsara, D. S., & Norman, M. L. 1992, ApJ, 393, 631
Bird, R., Stewart, W., & Lightfoot, E. 2002, Transport Phenomena (2nd. ed., New York: John Wiley and Sons)
Bliton, M., Rizza, E., Burns, J. O., Owen, F. N., & Ledlow, M. J. 1998, MNRAS, 301, 609
Bowman, M., Leahy, J. P., & Komissarov, S. S. 1996, MNRAS, 279, 899
Burns, J. O., & Owen, F. N. 1980, AJ, 85, 204
Cantó, J., & Raga, A. C. 1996, MNRAS, 280, 559
Canvin, J. R., & Laing, R. A. 2004, MNRAS, 350, 1342
De Young, D. S. 2002, The Physics of Extragalactic Radio Sources (Chicago: Chicago Univ. Press)
Fabbiano, G. 1989, ARA&A, 27, 87
Fanaroff, B. L., & Riley, J. M. 1974, MNRAS, 167, 31P
Goldstein, H., Poole, C., & Safko, J. 2002, Classical Mechanics (San Francisco: Addison-Wesley)
Goldstein, S. 1965, Modern Developments in Fluid Dynamics (New York: Dover)
Hardcastle, M. J., & Sakelliou, I. 2004, MNRAS, 349, 560
Hardee, P. E., Clarke, D. A., & Howell, D. A. 1995, ApJ, 441, 644
Hjellming, R. M., & Johnston, K. J. 1982, in IAU Symp. 97, Extragalactic Radio Sources, ed. D. S. Heeschen & C. M. Wade (Dordrecht: Reidel), 197
Hughes, W., & Brighton, J. 1967, Fluid Dynamics (New York: McGraw-Hill)
Icke, V. 1991, in Beams and Jets in Astrophysics, ed. P. A. Hughes (Cambridge: Cambridge Univ. Press), 232
Jaffe, W. J., & Perola, G. C. 1973, A&A, 26, 423
Kaiser, C. R., & Alexander, P. 1997, MNRAS, 286, 215
Laing, R. A., & Bridle, A. H. 2002a, MNRAS, 336, 1161
__________. 2002b, MNRAS, 336, 328
__________. 2004, MNRAS, 348, 1459
Laing, R. A., Parma, P., de Ruiter, H. R., & Fanti, R. 1999, MNRAS, 306, 513
Landau, L. 1987, Fluid Mechanics (2nd ed.; New York: Pergamon Press)
McCray, R. 1987, in Spectroscopy of Astrophysical Plasmas, ed. A. Dalgarno & D. Layzer (Cambridge: Cambridge Univ. Press), 255
Mendoza, S., Hernández, X., & Lee, W. H. 2005, RevMexAA, 41, 453
Mendoza, S., & Longair, M. S. 2001, MNRAS, 324, 149
__________. 2002, MNRAS, 331, 323
Miller, J. M., Ballantyne, D. R., Fabian, A. C., & Lewin, W. H. G. 2002, MNRAS, 335, 865
Murgia, M., Parma, P., de Ruiter, H. R., Bondi, M., Ekers,

R. D., Fanti, R., & Fomalont, E. B. 2001, A&A, 380, 102
Nakamura, M., Uchida, Y., & Hirose, S. 2001, NewA, 6, 61
Norman, M. L. 1996, in ASP Conf. Ser. 100, Energy Transport in Radio Galaxies and Quasars, ed. P. Hardee, A. H. Bridle, & J. Zensus (San Francisco: ASP), 319
Norman, M. L., Balsara, D., & O'Dea, C. 1994, BAAS, 26, 879
Odea, C. P. 1985, ApJ, 295, 80
Odea, C. P., & Owen, F. N. 1986, ApJ, 301, 841
Owen, F. N., Hardee, P. E., & Bignell, R. C. 1980, ApJ, 239, L11
Perley, R. A., Bridle, A. H., & Willis, A. G. 1984a, ApJS, 54, 291
Perley, R. A., Dreher, J. W., & Cowan, J. J. 1984b, ApJ, 285, L35
Raga, A. C., & Cantó, J. 1996, MNRAS, 280, 567
Reichardt, V. 1942, VDI-Forschungsheft, 414, 141
__________. 1951, Z. Angew. Math. Mech., 31, 208
Roettgering, H. J. A., van Ojik, R., Miley, G. K., Chambers, K. C., van Breugel, W. J. M., & de Koff, S. 1997, A&A, 326, 505
Schlichting, H. 1979, Boundary Layer Theory (New York: McGraw-Hill)
Sedov, L. I. 1959, Similarity and Dimensional Methods in Mechanics (New York: Academic Press)
Valtonen, M. J., & Kotilainen, J. 1989, AJ, 98, 117
Venkatesan, T. C. A., Batuski, D. J., Hanisch, R. J., & Burns, J. O. 1994, ApJ, 436, 67
Zaninetti, L. 1986, Phys. Fluids, 29, 332
__________. 1987, Phys. Fluids, 30, 612
__________. 1989, A&A, 221, 204

Lorenzo Zaninetti: Dipartimento di Fisica Generale, Università degli Studi di Torino, Via Pietro Giuria 1, 10125 Torino, Italy (zaninetti@ph.unito.it).